Research Article

Journal of Chemistry Letters
journal homepage: www.jchemlett.com
ISSN (online) 2717-1892 (print) 2821-0123

Do adsorbent pore size and specific surface area affect the kinetics of methyl orange aqueous phase adsorption?

Kingsley O. Iwuozor [a, *], Joshua O. Ighalo [b, c], Ebuka Chizitere Emenike [a], Chinenye Adaobi Igwegbe [b], Adewale George Adeniyi [c]

[a]*Department of Pure and Industrial Chemistry, Nnamdi Azikiwe University, P. M. B. 5025, Awka, Nigeria.*
[b]*Department of Chemical Engineering, Nnamdi Azikiwe University, P. M. B. 5025, Awka, Nigeria*
[c]*Department of Chemical Engineering, University of Ilorin, P. M. B. 1515, Ilorin, Nigeria*

ARTICLE INFO

Article history:
Received
Received in revised form
Accepted
Available online

Keywords:
Pore size
Kinetics
methyl orange
contact time
pseudo-second-order model

ABSTRACT

The kinetics of any adsorption reaction gives more information on the rate at which the adsorbate is taken up by the adsorbent, which is responsible for the residence time of the adsorbate uptake at the adsorbent-aqueous phase interface. This study was aimed at determining the effect of pore size as well as specific surface area (SSA) on the kinetics of the uptake of methyl orange (MO). The basis of the analysis was data on kinetic models sourced from recent literature. An ANOVA of the data revealed that statistical significance was achieved for SSA but not for pore size (at a significance level of 0.05). This called for a more theoretical perspective on the research data. The kinetics constant for micropores is far higher than for the two selected regimes of the mesopore. For the SSA, 100–10 m^2/g adsorbents had a higher mean value. This suggested that adsorbents in the SSA range had pore sizes that favoured rapid uptake. However, further studies will be needed to gain a better understanding of how SSA affects adsorption kinetics. The study also discussed the technical limitations that could arise due to the use of kinetic model linearisation.

1. Introduction

Adsorption is a very popular technique for the sequestration of pollutants such as dyes from the environment [1-4]. To obtain the optimum result in any adsorption study, the understanding of the following properties of the adsorbent is required: surface chemistry, hydrophilicity, physiochemical properties, proximate analysis, morphology, crystalline structure, and textural properties (pore size, pore volume, surface area, and pore surface) [5]. These characteristics are important in the selection of adsorbents for specific pollutants [6, 7]. The pore size of an adsorbent can be described as the gap or stretch of its pores. The pore size of adsorbents can be divided into three main groups as stated by the International Union of Pure and Applied Chemistry (IUPAC); micropores have pore sizes that are less than 2 nm, mesopores have pore sizes of 2-50 nm, and macropores have pore sizes greater than 50 nm [8-11]. The specific surface area (SSA) is also one of the most important properties of adsorbent material as it indicates the necessary active sites for adsorption because adsorption is a surface phenomenon [12-14]. The surface area is directly proportional to the adsorptive performance of the material [15, 16].

Adsorption modelling is a very important aspect of any adsorption study as it applies adsorption models for the interpretation of experimental data to obtain useful information that would aid in the understanding of process mechanisms, process equilibrium-dynamics, predicting answers to operational condition changes and optimizing the adsorption process [17, 18]. Common models used for understanding adsorption studies better are thermodynamic models, isotherm models, and kinetic models [3, 19-21].

The time at which equilibrium is obtained is an important feature of any adsorption study. The kinetics of any adsorption reaction gives more information on the rate at which the adsorbate is taken up by the adsorbent, which is responsible for the residence time of the adsorbate uptake at the adsorbent-aqueous phase interface [17]. The adsorption kinetics also gives more

* Corresponding author. e-mail: kingsleyiwuozor5@gmail.com

information on the mechanism as well as a pathway for the reaction [22, 23]. The most common kinetic models used in adsorption studies, which are classical models that fit adsorption data well even with non-linear methods, are the pseudo-first-order (PFO) and pseudo-second-order (PSO) models. The PFO model assumes that the adsorption process is dependent only on the concentration of adsorbate in the solution that is present at a specific time, while the PSO model assumes that adsorption is a complex physico-chemical process that is dependent on the concentration of the adsorbate present in the system as well as the number of active sites on the adsorbent [24-26].

Methyl Orange (MO) (IUPAC: Sodium 4-([4-(dimethylamino) phenyl]diazenyl) benzene-1-sulfonate) is a sulfonated azo anionic dye that is widely used as a pH indicator in acid titrations and as a textile dye [27-29]. It has a molecular formula of $C_{14}H_{12}N_3O_3NaS$ and a molecular weight of 327.34 g/mol. It is soluble in water and its density and melting point are 1.28 g/cm^3 and > 300 ℃ [30, 31]. The molecular size of MO is 1.19 nm × 0.68 nm × 0.37 nm. It has a dissociation constant (pKa) of 3.47 in water at 25 ℃ [32-34]. MO is a toxic compound that deteriorates water quality and has been banned for use in food products because it is a carcinogen and teratogen due to the presence of aromatic and –N=N- groups inherent in its structure, as shown in Figure 1 [34, 35]. It usually gets into the environment in large quantities through the effluent of textile industries. Different techniques have been utilized in the removal of MO from the environment. They include electrocoagulation [36-39], ozonation [40-42], biological treatment [43], photo-degradation [44-46], membrane processes [47], and adsorption [48-50]. Due to the low cost and efficacy of adsorption, it is considered one of the best methods for the removal of MO dye from the environment [51-53].

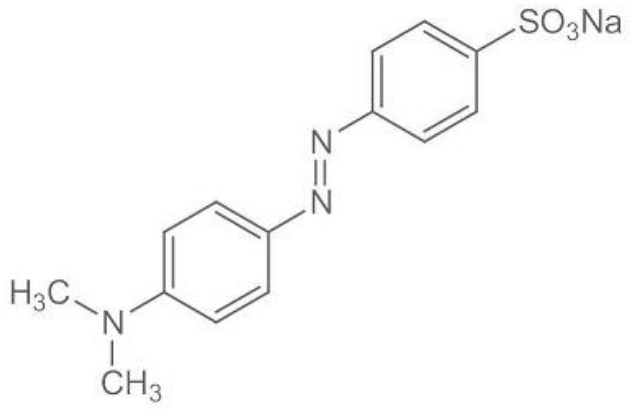

Figure 1. Chemical structure of methyl orange

This study is aimed at determining the relationship between pore size as well as specific surface area (SSA) on the kinetics of the uptake of methyl orange (MO) through the PFO and PSO kinetic models. Empirical findings obtained were analysed and juxtaposed to obtain observations. The reason for using MO in our study is its popularity as a pH indicator as well as a textile dye [54, 55]. The results of this study would be able to enable researchers to better understand the adsorption process of MO.

2. Results and Discussion

2.1Statistical analysis of the data

From Table 1, the pseudo-second-order kinetics was best-fit in most of the cases. Hence its kinetics constant (k_2) is the selected basis for this investigation. Firstly, before the data can be used for this analysis, we first need to verify if there is any statistical relationship between the pore size and specific surface area against the kinetic constant. This was done by the one-way ANOVA and descriptive statistics such as CV, R^2 and RMSE. From Table 2, statistical significance (at a threshold of Prob > F being 0.05) was achieved for SSA but not for pore size. What this simply means is that a holistic consideration of the data revealed specific trends between SSA and the kinetics constant while this was not so for the case of pore size. It is also unsurprising that the descriptive statistics are also correspondingly poorer for pore size. This does not however invalidate the data since the statistical significance only verifies if the results in the dataset are due to chance or some specific factors. A more theoretical perspective will be needed to properly consider the data.

Table 2. One-way ANOVA and descriptive statistics of the factors on k_2

Result	**SSA**
F – value (One-way ANOVA)	4.33×10^{10}
Prob > F (One-way ANOVA)	2.31×10^{-11}
Coefficient of determination (R^2)	1.000
Coefficient of variance (CV)	3.79×10^{-5}
RMSE	0.00752

2.2 Theoretical consideration of the effect of pore size on MO adsorption kinetics

Empirical evidence cannot be summarily dismissed due to a lack of a statistical relationship. Statistics try to evaluate trends based on a holistic computation of the dataset. This does not consider some known theoretical understanding of adsorption. For this case, we are considering the 2 nm pore size threshold. This will be used to differentiate between the micropore and the mesopore. Based on this, we can then summarise the data as shown in Table 3. Considering magnitudes, it is observed that the kinetics for micropores is far higher than for the two selected regimes of the mesopore. We believe this is a bias induced by the uncharacteristic results obtained by Chaukura, et al. [56] for Fe_2O_3/biochar adsorption of MO. If this value is excluded, we still obtain a mean k_2 value of 34.1 which is still significantly higher than for mesopores. The molecular size of MO is 1.19 nm × 0.68 nm × 0.37 nm. This dimension suggests that it would quickly fill up a pore with an average diameter of 2 nm as opposed to

larger mesopores. This quickness is what is captured by the rate constant.

Table 3. Variation of pore size with mean K_2 values for MO adsorption

Regime	Pore size (nm)	Mean K_2 (g/mg.min)
Mesoporous	50 – 10	0.3659
Mesoporous	10 – 2	0.6788
Microporous	< 2	919.3

2.3.Theoretical consideration of the effect of SSA on MO adsorption kinetics

In this section, we investigate the possible effects of SSA on MO adsorption kinetics. A simple summary of the results is presented in Table 4. For the SSA, 100 – 10 m^2/g adsorbents had a higher mean k_2 value. This suggests that adsorbents in the SSA range had pore sizes that favoured rapid uptake (which we have already observed to be micropores). The SSA of a material is only closely related to its total pore volume. Pore diameters are controlled more by the method and parameters of adsorbent preparation than by the intrinsic nature of the feedstock. Hence, further studies will be needed to gain a better understanding of how SSA affects the adsorption kinetics (if at all it does).

Table 4. Variation of SSA with mean K_2 values for MO adsorption

SSA (m^2/g)	Mean K_2 (g/mg.min)
3000 – 1000	17.49
1000 – 100	12.52
100 – 10	460.5
10 – 0	0.1616

2.4.Technical issues with kinetics modelling

In this section, we discuss the technical issues around the modelling of adsorption kinetics, albeit from a mathematical perspective. In Table 1, we reported the technique used by various studies for modelling adsorption. A majority of the studies used the linear modelling technique while others employed non-linear modelling. Tran, et al. [5] explained that the kinetics of adsorption can be very rapid. In some cases, over 90% of the adsorbate can be removed within the first 5 minutes of the process. Most experiments usually employed a protracted contact time because the adsorption process becomes significantly less rapid as equilibrium is approached. Simonin [57] has explained that serious biases that favour the PSO model are created because of this extended portion of the contact time when kinetics is slow and equilibrium is close. Such vast differences in adsorption kinetics can be difficult to capture by a linearised model. This led to the issues raised by Lima, et al. [58]. Lima, et al. [58] observed that researchers seem too confident in employing linear techniques because of their perceived similarity with non-linear modelling when comparing their R^2 and adjusted R^2. This did not take into cognisance the dissimilarities and inconsistencies in the obtained rate constants [59-64]. In some scenarios, studies with PFO as best-fits were erroneously assigned as having PSO as best-fit. It is by consequence not surprising that most of the studies in Table 1 have the PSO as best-fit. Besides the use of just the R^2 for determining goodness of fit, Aniagor, et al. [25] recommended including other accuracy statistics in making this decision (which are still not commonly employed in literature in this respect). Increment in the degree of freedom of a given kinetics data set will unfairly favour the model fit. Hence this suggestion.

3. Experimental

3.1.Data Collection and description

For our study, published works of literature on the adsorption of Methyl Orange were obtained from the Google Scholar search engine. The search was restricted to articles published in the past five years (2016 - 2021) and which reported the pore size of the various adsorbents used. Based on the nature of the data, adsorbent of macropores size is unavailable for MO adsorption hence the study would focus more on micropore versus mesopore. Data on SSA was also added from articles where it was reported as shown in Table 1. The kinetic models used in this study was restricted to the PFO and the PSO models. The K values of the models were reported based on which of them was best-fit from the authors' modelling study. The most widely reported index of kinetic modelling accuracy (being the coefficient of determination, R^2) was also reported. The modelling techniques were reported too, L being for linear modelling and NL being for non-linear modelling.

3.2.Research Problem

To verify the effect of pore size on adsorption kinetics, the data were analysed in a variety of ways. The key goal was to evaluate how pore size and SSA relates to the kinetic constants. The kinetic constant was used as the basis of the investigation because it is in the true sense an empirical constant. Hence comparison can be made across studies using it which extricates other adsorption factors. Furthermore, only methyl orange was used because it also helps to narrow down the factors by eliminating the effects of adsorbate properties on the solution chemistry. The study will try to evaluate if there was there a relationship from empirical investigations between pore size and SSA against MO uptake kinetics. The study also discusses the influence of the modelling technique (whether linear or non-linear) on adsorption kinetics [65].

Table 1. Data on MO uptake pore sizes, SSA and kinetic constants

Adsorbent Name	Average Pore Size (nm)	SSA (m^2/g)	K_1 (1/min)	R^2	K_2 (g/mg.min)	R^2	Modelling type	Ref.
ZnO nanostructure	51.60	7.780	-	-	-	-	-	[66]
LDH/Fe_3O_4/polyvinyl alcohol	42.00	87.00	-	-	-	0.9750	L	[67]
Chitosan/ethylene glycol diglycidyl ether biofilm	27.62	0.820	-	-	0.0006	0.9900	NL	[68]
Goethite/chitosan beads	26.18	17.81	-	-	0.0003	0.9965	-	[69]
Flower-like NiAl LDH	23.30	133.0	-	-	0.0058	0.9990	NL	[70]
Starch-modified ZnMgAl LDH	23.10	76.80	-	-	0.00007	0.9999	NL	[71]
Biochar from waste walnut shells/TiO_2	22.70	66.06	-	-	-	-	-	[72]
Polyethyleneimine-modified persimmon tannin	19.54	8.130	-	-	0.0047	0.9994	L	[73]
$[Cu(L)_2(H_2O)H_2(Cu(L)_2(P_2Mo_5O_{23})].4H_2O/Fe_3O_4$	19.43	-	-	-	-	-	-	[74]
Au/Cu_2O	18.30	16.00	-	-	-	-	-	[75]
Bi_2O_3/TiO_2/powdered AC	17.60	83.30	-	-	5.9620	1.0000	-	[76]
Chitosan beads	16.69	10.81	-	-	0.0003	0.9939	NL	[69]
Co_3O_4 nanocube/polyaniline	15.57	43.00	-	-	0.0006	0.9990	L	[77]
Blast furnace slag acid-alkaline precipitate	15.40	3.450	-	-	0.1590	1.0000	L	[78]
Immobilized polyaniline	14.70	8.500	-	-	0.0800	0.9900	L	[79]
Graphene oxide/NiFe LDH	14.60	145.0	-	-	0.0006	0.9990	NL	[80]
Polyaniline nano-adsorbent	13.82	10.44	-	-	0.0483	0.9447	NL	[81]
Polyanilined-based nanoadsorbent	13.82	10.34	-	-	-	-	-	[82]
Fly ash	13.54	1.180	-		-	-	-	[83]
Trimeric surfactant-modified NA montmorillonite	13.41	7.750	-	-	1.0230	0.9988	L	[84]
Mesoporous ZIF-67/LDH	13.24	172.3	-	-	0.0002	0.9998	L	[85]
Silver NP/zeolite X	12.42	552.6	0.3050	0.9820	-	-	L	[86]
Hydrotalcite-like modified bentonite	12.13	83.24	-	-	0.0050	0.9990	NL	[87]
Magnetic lignin-based CNPs	12.00	82.80	-	-	0.0008	0.9992	L	[88]
CuO NPs	11.61	6.188	-	-	0.0244	0.9980	L	[89]
NiFe LDH nanoflakes/montmorillonite	10.70	103.9	-	-	0.0017	0.9980	NL	[90]
Goethite	10.24	4.370	-	-	0.0004	0.9953	NL	[69]
Calcium ferrite/zirconia	10.18	95.32	-	-	0.0001	1.0000	L	[91]
CuO nanostructures	9.000	24.10	-	-	-	-	-	[92]
MgAL-LDHs nanosheets	8.870	65.94	-	-	-	-	-	[93]
Dimeric surfactant-modified NA montmorillonite	8.830	10.72	-	-	1.4510	0.9889	L	[84]
Date palm ash/MgAl-LDH	8.730	140.7	-	-	0.0013	0.9990	NL	[94]
Catechol/amine resin	8.590	13.13		-	0.0007	0.9997	L	[95]
CoFe LDH	8.400	108.8	-	-	-	-	-	[96]
CuAl LDH	7.358	-	-	-	-	-	-	[97]
Cetyltrimethylammonium bromide/H_2O_2-clay	6.804	21.16	-	-	0.0250	0.9999	L	[98]
Bismuth nitrate NP	5.850	5.290	-	-	-	0.9998	L	[99]
Chitosan/$Fe(OH)_3$ beads	5.710	10.20	-	-	0.0068	0.9998	L	[100]
Manganous(ll) ions-based MOF	5.619	-	-	-	-	-	-	[101]
Mesoporous carbon	5.300	2944	-	-	0.0002	1.0000	L	[102]
TiO_2/aluminosilicate zeolite (ZSM-5)	5.200	1151	-	-		0.9994	L	[103]
Mesoporous carbon nanofibers	5.000	392.3	-	-	0.0002	0.9967	L	[104]
ZnO/polyaniline	5.000	63.17	-	-	0.0012	0.9990	L	[105]
γ-Fe_2O_3/2C nanocomposites	4.965	394.1	-	-	0.0024	0.9996	NL	[106]
MOF-derived nanoporous carbon	4.770	1731	-	-	0.0011	0.9937	NL	[107]
Cd-zeolite imidazolate framework (Cd-ZIF-8)	4.700	1281	-	-	0.0080	0.9900	NL	[108]
Nitrogen-doped porous carbon	4.200	1259	-	-	-	-	-	[109]
Porous ZnO spheres	4.150	114.6	-	-	-	-	-	[110]
Al-doped CNTs	3.820	118.8	-	-	0.0044	0.9990	NL	[111]
Stone-like NiAl LDH	3.800	90.00	-	-	0.0015	0.9900	NL	[70]
Nanoporous carbon	3.700	814.0	-	-	0.1490	0.0760	L	[112]
NiO NPs	3.492	78.37	-	-	0.0002	0.9900	L	[89]
AC from sugarcane mills boiler residue	3.372	1073		-	0.0001	0.9923	L	[113]
CoAl/Cl LDH	3.344	19.70	-	-	0.0002	0.9890	NL	[114]
Mesoporous MCM-41	3.280	1451	-	-	0.0057	0.9995	L	[115]
p-CNTs/N,N-diethylethanol ammonium chloride	3.009	169.7	-	-	0.0001	0.9900	L	[116]
Nitrogen-doped mesoporous carbon	3.000	968.0	-	-	-	-	-	[117]
NDA88 MOF/Cu	2.990	370.4	-	-	-	-	-	[118]
Calcinated organic matter-rich clays from Egypt	2.988	48.32	-	-	0.0370	0.9999	L	[119]
Organic matter-rich clays from Egypt	2.930	59.14	-	-	0.0940	1.0000	L	[119]
Fe_2O_3/Mn_3O_4 magnetic nanocomposites	2.870	178.3	-	-	0.0003	0.9998	L	[120]
Copper sulphide NPs/AC	2.840	1286	-	-	0.0300	0.9900	L	[121]
Magnetic nanoporous Fe/MCM-41	2.840	1216	-	-	0.0057	0.9995	L	[115]
Ni-Co-S/hexadecyltrimethyl ammonium bromide	2.780	12.73	-	-	0.0237	0.9962	NL	[122]
Fe_3O_4/AC	2.750	1200	-	-	18.950	0.9999	NL	[123]
Organosilica	2.700	10.00	-		0.0001	0.9860	NL	[124]
AC from popcorn	2.580	3291	-	-	-	-	-	[125]
AC from coconut shell	2.520	1640	-	-	0.2266	0.9959	L	[126]
$AgGaO_2$ nanocomposites	2.500	23.35	-	-	-	-	-	[127]
p-CNTs/chlorine chloride	2.413	197.8	-	-	0.00003	0.9900	L	[116]
Nickel hydroxide catalysts	2.400	87.00	-	-	-	-	-	[128]
Nano ZnO/mesoporous silica	2.176	849.0	0.0182	0.9931	-	-	L	[129]

Chitosan/Al_2O_3/Fe_3O_4	2.122	21.87	-	-	0.0173	0.9997	L	[130]
Non-functionalized CNTs (p-CNTs)	2.049	123.5	-	-	0.00004	0.9900	L	[116]
TiO_2/slag-made calcium silicate	2.030	149.0	-	-	-	-	-	[131]
Carbon nanostructure from Bengal gram bean husk	1.940	1710	-	-	00243	1.0000	L	[132]
Pomelo peel-derived porous carbon	1.920	1892	-	-	0.0022	0.9939	L	[133]
Polyaniline/AC	1.840	36.00	-	-	0.0002	0.9996	L	[134]
Polyvinylene fluoride/PEDOT mats	1.807	5.691	-	-	0.0004	0.9990	NL	[135]
Mg NP/modified nanosized Si_2-Al_2O_3	1.800	101.0	-	-	0.1690	0.9990	NL	[136]
NiFe LDH	1.800	17.85	-	0.9998	-	-	L	[137]
Nitrogen-doped nanoporous carbon	1.730	1152	-	-	0.0810	0.9980	L	[138]
UiO-66 MOF	1.700	1276	-	-	0.0062	0.9990	L	[139]
Fe_2O_3/biochar	1.700	15.30	-	-	12427	0.9990	L	[56]
Ag-N-ZnO/coconut husk AC	1.350	472.0	-	-	0.0037	0.9862	NL	[140]
TiO_2/pure calcium silicate	1.340	126.0	-	-	-	-	-	[131]
Tungstosilisic acid/zeolites	1.000	362.0	-	-	-	-	-	[141]
Activated biochar from pemelo peel waste	0.940	75.32	-	-	0.0007	0.9840	L	[142]
Al-doped MOF/grapheme oxide	0.600	1309	-	-	0.0060	1.000	NL	[143]
Cd-based MOF	0.246	384.0	-	-	200.00	0.9990	L	[144]
N-acyl thiolated chitosan	0.214	10.00	-	-	0.0150	0.9999	NL	[145]
Salecan polyssacharides	0.109	-	-	-	-	0.9941	L	[146]
Mesoporous MCM-41/microfiltration membrane	0.0002	1451	-	-	0.0078	0.9998	L	[147]

3.3.Data. analysi

Statistical analysis of the data was done using one-way analysis of variance (ANOVA) and descriptive statistics such as coefficient of variance (CV), coefficient of determination (R^2) and root mean square error (RMSE). This analysis was done using Origin Pro 2017 (OriginLab Co., Wellesley, MA, USA). Other analyses for the determination of means was done using Microsoft excel 2016 (Microsoft Inc., Redmond, WA, USA).

4. Conclusion

Some unique observations were derived from this study, albeit MO adsorption. ANOVA of the data revealed that statistical significance (at a threshold of Prob> F of 0.05) was achieved for SSA but not for pore size. This does not, however, invalidate the data since the statistical significance only verifies if the results in the dataset are due to chance or some specific factors, thereby requiring a more theoretical perspective. It was discovered that the kinetics of micropores are far greater than those of the two selected mesopore regimes.Based on the molecular size of MO, the compound would quickly fill up a pore with an average diameter of 2 nm as opposed to larger mesopores. This quickness is what is captured by the rate constant. For the SSA, 100−10 m2/g adsorbents had a higher mean value. This suggested that adsorbents in the SSA range had pore sizes that favour rapid uptake (which we have already observed to be micropores). However, further studies will be needed to gain a better understanding of how SSA affects the adsorption kinetics (if at all it does).

References

[1] Zhul-quarnain A, Ogemdi IK, Modupe I, Gold E, Chidubem EE. Adsorption of malachite green dye using orange peel. Journal of Biomaterials 2018;2(2):31-40.

[2] Ogunlalu O, Oyekunle IP, Iwuozor KO, Aderibigbe AD, Emenike EC. Trends in the mitigation of heavy metal ions from aqueous solutions using unmodified and chemically-modified agricultural waste adsorbents. Current Research in Green and Sustainable Chemistry 2021;4:18. https://doi.org/https://doi.org/10.1016/j.crgsc.2021.100188.

[3] Ogemdi IK. Removal of Heavy Metals from Their Solution Using Polystyrene Adsorbent (Foil Take-Away Disposable Plates).

[4] Iwuozor KO, Oyekunle IP, Oladunjoye IO, Ibitogbe EM, Olorunfemi TS. A Review on the Mitigation of Heavy Metals from Aqueous Solution using Sugarcane Bagasse. SugarTech 2021;23:19. https://doi.org/10.1007/s12355-021-01051-w.

[5] Tran HN, You S-J, Hosseini-Bandegharaei A, Chao H-P. Mistakes and inconsistencies regarding adsorption of contaminants from aqueous solutions: a critical review. Water research 2017;120:88-116.

[6] Mangun C, Daley M, Braatz R, Economy J. Effect of pore size on adsorption of hydrocarbons in phenolic-based activated carbon fibers. Carbon 1998;36(1-2):123-9.

[7] Iwuozor KO, Gold EE. Physico-chemical parameters of industrial effluents from a brewery industry in Imo state, Nigeria. Advanced Journal of Chemistry-Section A 2018;1(2):66-78.

[8] Zhang X, Li A, Jiang Z, Zhang Q. Adsorption of dyes and phenol from water on resin adsorbents: effect of adsorbate size and pore size distribution. Journal of hazardous materials 2006;137(2):1115-22.

[9] Aysan H, Edebali S, Ozdemir C, Karakaya MC, Karakaya N. Use of chabazite, a naturally abundant zeolite, for the investigation of the adsorption kinetics and mechanism of methylene blue dye. Microporous and Mesoporous Materials 2016;235:78-86.

[10] Lorenc-Grabowska E, Diez MA, Gryglewicz G. Influence of pore size distribution on the adsorption of phenol on PET-based activated carbons. Journal of colloid and interface science 2016;469:205-12.

[11] Iwuozor KO, Ighalo JO, Ogunfowora LA, Adeniyi AG, Igwegbe CA. An Empirical Literature Analysis of Adsorbent Performance for Methylene Blue Uptake from Aqueous Media. Journal of Environmental Chemical Engineering 2021:105658.

[12] Lee SB, Shin H, Ryu DD, Mandels M. Adsorption of cellulase on cellulose: effect of physicochemical properties of cellulose on adsorption and rate of hydrolysis. Biotechnology and Bioengineering 1982;24(10):2137-53.

[13] Yin G, Song X, Tao L, Sarkar B, Sarmah AK, Zhang W, et al. Novel Fe-Mn binary oxide-biochar as an adsorbent for removing Cd (II) from aqueous solutions. Chemical Engineering Journal 2020;389:124465.
[14] de la Luz-Asunción M, Pérez-Ramírez EE, Martínez-Hernández AL, Castano VM, Sánchez-Mendieta V, Velasco-Santos C. Non-linear modeling of kinetic and equilibrium data for the adsorption of hexavalent chromium by carbon nanomaterials: Dimension and functionalization. Chinese Journal of Chemical Engineering 2019;27(4):912-9.
[15] Lv L, Huang Y, Cao D. Nitrogen-doped porous carbons with ultrahigh specific surface area as bifunctional materials for dye removal of wastewater and supercapacitors. Applied Surface Science 2018;456:184-94.
[16] Ogemdi IK. Properties and Uses of Colloids: A Review. Colloid and Surface Science 2019;4(2):24.
[17] Unuabonah EI, Omorogie MO, Oladoja NA. Modeling in adsorption: fundamentals and applications. Composite Nanoadsorbents: Elsevier; 2019, p. 85-118.
[18] Iwuozor KO, Abdullahi TA, Ogunfowora LA, Emenike EC, Oyekunle IP, Gbadamosi FA, et al. Mitigation of levofloxacin from aqueous media by adsorption: a review. Sustainable Water Resources Management 2021;7(6):1-18.
[19] Balarak D, Zafariyan M, Igwegbe CA, Onyechi KK, Ighalo JO. Adsorption of Acid Blue 92 Dye from Aqueous Solutions by Single-Walled Carbon Nanotubes: Isothermal, Kinetic, and Thermodynamic Studies. Environmental Processes 2021;8(2):869-88.
[20] Ighalo JO, Adeniyi AG. Statistical modelling and optimisation of the biosorption of Cd (II) and Pb (II) onto dead biomass of Pseudomonas aeruginosa. Chemical Product and Process Modeling 2021;16(1).
[21] Ogemdi IK. Heavy Metal Concentration of Aphrodisiac Herbs Locally Sold in the South-Eastern Region of Nigeria. Pharmaceutical Science and Technology 2019;3(1):22.
[22] de Souza EC, Pimenta AS, da Silva AJF, do Nascimento PFP, Ighalo JO. Oxidized eucalyptus charcoal: a renewable biosorbent for removing heavy metals from aqueous solutions. Biomass Conversion and Biorefinery 2021:1-15.
[23] Ali RM, Hamad HA, Hussein MM, Malash GF. Potential of using green adsorbent of heavy metal removal from aqueous solutions: adsorption kinetics, isotherm, thermodynamic, mechanism and economic analysis. Ecological Engineering 2016;91:317-32.
[24] Igwegbe CA, Oba SN, Aniagor CO, Adeniyi AG, Ighalo JO. Adsorption of ciprofloxacin from water: a comprehensive review. Journal of Industrial and Engineering Chemistry 2020.
[25] Aniagor CO, Igwegbe CA, Ighalo JO, Oba SN. Adsorption of doxycycline from aqueous media: A review. Journal of Molecular Liquids 2021;334:116124.
[26] Ighalo JO, Ajala OJ, Umenweke G, Ogunniyi S, Adeyanju CA, Igwegbe CA, et al. Mitigation of clofibric acid pollution by adsorption: a review of recent developments. Journal of Environmental Chemical Engineering 2020:104264.
[27] Hanafi MF, Sapawe N. Performance of nickel catalyst toward photocatalytic degradation of methyl orange. Materials Today: Proceedings 2020;31:257-9.
[28] Hanafi MF, Sapawe N. A review on the water problem associate with organic pollutants derived from phenol, methyl orange, and remazol brilliant blue dyes. Materials Today: Proceedings 2020;31:A141-A50.
[29] Iwuozor KO, Ighalo JO, Emenike EC, Ogunfowora LA, Igwegbe CA. Adsorption of methyl orange: A review on adsorbent performance. Current Research in Green and Sustainable Chemistry 2021;4:16. https://doi.org/https://doi.org/10.1016/j.crgsc.2021.100179.
[30] Youssef NA, Shaban SA, Ibrahim FA, Mahmoud AS. Degradation of methyl orange using Fenton catalytic reaction. Egyptian Journal of Petroleum 2016;25(3):317-21.
[31] Information NCfB. PubChem Compound Summary for CID 23673835, Methyl orange. 2021.
[32] Trabelsi H, Khadhraoui M, Hentati O, Ksibi M. Titanium dioxide mediated photo-degradation of methyl orange by ultraviolet light. Toxicological & Environmental Chemistry 2013;95(4):543-58.
[33] Huang J. Molecular sieving effect of a novel hyper-cross-linked resin. Chemical Engineering Journal 2010;165(1):265-72.
[34] Wu L, Liu X, Lv G, Zhu R, Tian L, Liu M, et al. Study on the adsorption properties of methyl orange by natural one-dimensional nano-mineral materials with different structures. Scientific reports 2021;11(1):1-11.
[35] Ashok V, Agrawal N, Esteve-Romero J, Bose D, Dubey NP. Detection of Methyl Orange in Saffron and Other Edibles Using Direct Injection Micellar Liquid Chromatography. Food Analytical Methods 2017;10(1):269-76.
[36] Irki S, Ghernaout D, Naceur MW. Decolourization of methyl orange (MO) by electrocoagulation (EC) using iron electrodes under a magnetic field (MF). Desalination and Water Treatment 2017;79:368-77.
[37] Irki S, Ghernaout D, Naceur MW, Alghamdi A, Aichouni M. Decolorizing Methyl Orange by Fe-Electrocoagulation Process—A Mechanistic Insight. International Journal of Environmental Chemistry 2018;2:18-28.
[38] Irki S, Ghernaout D, Naceur MW, Alghamdi A, Aichouni M. Decolorization of methyl orange (MO) by electrocoagulation (EC) using iron electrodes under a magnetic field (MF). II. Effect of connection mode. World Journal of Applied Chemistry 2018;3:56-64.
[39] Iwuozor KO. Prospects and Challenges of Using Coagulation-Flocculation method in the treatment of Effluents. Advanced Journal of Chemistry-Section A 2019;2(2):105-27.
[40] Zhang H, Duan L, Zhang D. Decolorization of methyl orange by ozonation in combination with ultrasonic irradiation. Journal of hazardous materials 2006;138(1):53-9.
[41] Chen L-C. Effects of factors and interacted factors on the optimal decolorization process of methyl orange by ozone. Water Research 2000;34(3):974-82.
[42] Lee M-E, Kim J-E, Chung JW. Effect of Operating Parameters on Methyl Orange Removal in Catalytic Ozonation. Journal of Korean Society of Environmental Engineers 2017;39(7):412-7.
[43] Almaamary E, Abdullah S, Hasan H, Ismail N, Ab Rahim R, Idris M. Plant-assisted remediation of wastewater contaminated with methyl orange using Scirpus grossus. Journal of Environmental Biology 2019;40(3):515-23.

[44] Li W, Li D, Lin Y, Wang P, Chen W, Fu X, et al. Evidence for the active species involved in the photodegradation process of methyl orange on TiO2. The Journal of Physical Chemistry C 2012;116(5):3552-60.
[45] Arabatzis I, Stergiopoulos T, Bernard M, Labou D, Neophytides S, Falaras P. Silver-modified titanium dioxide thin films for efficient photodegradation of methyl orange. Applied Catalysis B: Environmental 2003;42(2):187-201.
[46] Yan S, Li Z, Zou Z. Photodegradation of rhodamine B and methyl orange over boron-doped g-C3N4 under visible light irradiation. Langmuir 2010;26(6):3894-901.
[47] Liu J, Xiong J, Tian C, Gao B, Wang L, Jia X. The degradation of methyl orange and membrane fouling behavior in anaerobic baffled membrane bioreactor. Chemical Engineering Journal 2018;338:719-25.
[48] Yao Y, Bing H, Feifei X, Xiaofeng C. Equilibrium and kinetic studies of methyl orange adsorption on multiwalled carbon nanotubes. Chemical Engineering Journal 2011;170(1):82-9.
[49] Mohammadi N, Khani H, Gupta VK, Amereh E, Agarwal S. Adsorption process of methyl orange dye onto mesoporous carbon material–kinetic and thermodynamic studies. Journal of colloid and interface science 2011;362(2):457-62.
[50] Mittal A, Malviya A, Kaur D, Mittal J, Kurup L. Studies on the adsorption kinetics and isotherms for the removal and recovery of Methyl Orange from wastewaters using waste materials. Journal of hazardous materials 2007;148(1-2):229-40.
[51] Balarak D, Mahdavi Y, Bazrafshan E, Mahvi AH. Kinetic, isotherms and thermodynamic modeling for adsorption of Acid Blue 92 (AB92) from aqueous solution by modified Azolla filicoloides. Fresenius Environmental Bulletin 2016;25(5):1322-31.
[52] Azarpira H, Balarak D. Biosorption of acid orang 7 using dried cyperus rotundus: Isotherm studies and error functions. International Journal of ChemTech Research 2016;9(9):543-9.
[53] Balarak D, Mostafapour F, Joghataei A. Adsorption of Acid Blue 225 dye by Multi Walled Carbon Nanotubes: Determination of equilibrium and kinetics parameters. Der Pharma Chemica 2016;8(8):138-45.
[54] do Vale-Júnior E, da Silva DR, Fajardo AS, Martínez-Huitle CA. Treatment of an azo dye effluent by peroxi-coagulation and its comparison to traditional electrochemical advanced processes. Chemosphere 2018;204:548-55.
[55] Chen H, Zhao J, Wu J, Dai G. Isotherm, thermodynamic, kinetics and adsorption mechanism studies of methyl orange by surfactant modified silkworm exuviae. Journal of hazardous materials 2011;192(1):246-54.
[56] Chaukura N, Murimba EC, Gwenzi W. Synthesis, characterisation and methyl orange adsorption capacity of ferric oxide–biochar nano-composites derived from pulp and paper sludge. Applied Water Science 2016;7(5):2175-86. https://doi.org/10.1007/s13201-016-0392-5.
[57] Simonin J-P. On the comparison of pseudo-first order and pseudo-second order rate laws in the modeling of adsorption kinetics. Chem Eng J 2016;300:254-63.
[58] Lima EC, Sher F, Guleria A, Saeb MR, Anastopoulos I, Tran HN, et al. Is one performing the treatment data of adsorption kinetics correctly? Journal of Environmental Chemical Engineering 2021;9(2):104813.
[59] Oba SN, Ighalo JO, Aniagor CO, Igwegbe CA. Removal of ibuprofen from aqueous media by adsorption: A comprehensive review. Sci Total Environ 2021;780:146608. https://doi.org/http://dx.doi.org/10.1016/j.scitotenv.2021.146608.
[60] Onyekachi OE, Iwuozor KO. Mechanical and Water Absorption Properties of Polymeric Compounds. American Journal of Mechanical and Materials Engineering 2019;3(2):36-46.
[61] Siadati SA, Rezazadeh S. Switching behavior of an actuator containing germanium, silicon-decorated and normal C20 fullerene. Chemical Review and Letters 2018;1(2):77-81.
[62] Vessally E, Siadati SA, Hosseinian A, Edjlali L. Selective sensing of ozone and the chemically active gaseous species of the troposphere by using the C20 fullerene and graphene segment. Talanta 2017;162:505-10.
[63] Siadati SA, Vessally E, Hosseinian A, Edjlali L. Possibility of sensing, adsorbing, and destructing the Tabun-2D-skeletal (Tabun nerve agent) by C20 fullerene and its boron and nitrogen doped derivatives. Synthetic Metals 2016;220:606-11.
[64] Siadati SA, Kula K, Babanezhad E. The possibility of a two-step oxidation of the surface of C20 fullerene by a single molecule of nitric (V) acid, initiate by a rare [2+ 3] cycloaddition. Chemical Review and Letters 2019;2:2-6.
[65] Ighalo JO, Iwuozor KO, Igwegbe CA, Adeniyi AG. Verification of Pore Size Effect on Aqueous-Phase Adsorption Kinetics: A Case Study of Methylene Blue. Colloids and Surfaces A: Physicochemical and Engineering Aspects 2021:127119.
[66] Nasrollahzadeh MS, Hadavifar M, Ghasemi SS, Arab Chamjangali M. Synthesis of ZnO nanostructure using activated carbon for photocatalytic degradation of methyl orange from aqueous solutions. Applied Water Science 2018;8(4). https://doi.org/10.1007/s13201-018-0750-6.
[67] Mallakpour S, Hatami M. An effective, low-cost and recyclable bio-adsorbent having amino acid intercalated LDH@Fe3O4/PVA magnetic nanocomposites for removal of methyl orange from aqueous solution. Applied Clay Science 2019;174:127-37. https://doi.org/10.1016/j.clay.2019.03.026.
[68] Jawad AH, Mamat NFH, Hameed BH, Ismail K. Biofilm of cross-linked Chitosan-Ethylene Glycol Diglycidyl Ether for removal of Reactive Red 120 and Methyl Orange: Adsorption and mechanism studies. Journal of Environmental Chemical Engineering 2019;7(2):102965. https://doi.org/10.1016/j.jece.2019.102965.
[69] Munagapati VS, Yarramuthi V, Kim D-S. Methyl orange removal from aqueous solution using goethite, chitosan beads and goethite impregnated with chitosan beads. Journal of Molecular Liquids 2017;240:329-39. https://doi.org/10.1016/j.molliq.2017.05.099.
[70] El Hassani K, Beakou BH, Kalnina D, Oukani E, Anouar A. Effect of morphological properties of layered double hydroxides on adsorption of azo dye Methyl Orange: A comparative study. Applied Clay Science 2017;140:124-31. https://doi.org/10.1016/j.clay.2017.02.010.
[71] Tao X, Liu D, Cong W, Huang L. Controllable synthesis of starch-modified ZnMgAl-LDHs for adsorption property improvement. Applied Surface Science 2018;457:572-9. https://doi.org/10.1016/j.apsusc.2018.06.264.

[72] Lu L, Shan R, Shi Y, Wang S, Yuan H. A novel TiO2/biochar composite catalysts for photocatalytic degradation of methyl orange. Chemosphere 2019;222:391-8. https://doi.org/10.1016/j.chemosphere.2019.01.132.

[73] Li X, Wang Z, Ning J, Gao M, Jiang W, Zhou Z, et al. Preparation and characterization of a novel polyethyleneimine cation-modified persimmon tannin bioadsorbent for anionic dye adsorption. Journal of environmental management 2018;217:305-14. https://doi.org/10.1016/j.jenvman.2018.03.107.

[74] Fang N, Ji Y-M, Li C-Y, Wu Y-Y, Ma C-G, Liu H-L, et al. Synthesis and adsorption properties of [Cu(L)2(H2O)]H2[Cu(L)2(P2Mo5O23)]·4H2O/Fe3O4 nanocomposites. RSC Advances 2017;7(41):25325-33. https://doi.org/10.1039/c7ra02133j.

[75] Wu X, Cai J, Li S, Zheng F, Lai Z, Zhu L, et al. Au@Cu2O stellated polytope with core-shelled nanostructure for high-performance adsorption and visible-light-driven photodegradation of cationic and anionic dyes. J Colloid Interface Sci 2016;469:138-46. https://doi.org/10.1016/j.jcis.2016.01.064.

[76] Shang Y, Li X, Yang Y, Wang N, Zhuang X, Zhou Z. Optimized photocatalytic regeneration of adsorption-photocatalysis bifunctional composite saturated with Methyl Orange. J Environ Sci (China) 2020;94:40-51. https://doi.org/10.1016/j.jes.2020.03.044.

[77] Shahabuddin S, Sarih NM, Mohamad S, Atika Baharin SN. Synthesis and characterization of Co3O4 nanocube-doped polyaniline nanocomposites with enhanced methyl orange adsorption from aqueous solution. RSC Advances 2016;6(49):43388-400. https://doi.org/10.1039/c6ra04757b.

[78] Gao H, Song Z, Zhang W, Yang X, Wang X, Wang D. Synthesis of highly effective absorbents with waste quenching blast furnace slag to remove Methyl Orange from aqueous solution. J Environ Sci (China) 2017;53:68-77. https://doi.org/10.1016/j.jes.2016.05.014.

[79] Bahrudin NN, Nawi MA, Ismail WINW. Physical and adsorptive characterizations of immobilized polyaniline for the removal of methyl orange dye. Korean Journal of Chemical Engineering 2018;35(7):1450-61. https://doi.org/10.1007/s11814-018-0052-6.

[80] Zheng Y, Cheng B, You W, Yu J, Ho W. 3D hierarchical graphene oxide-NiFe LDH composite with enhanced adsorption affinity to Congo red, methyl orange and Cr(VI) ions. J Hazard Mater 2019;369:214-25. https://doi.org/10.1016/j.jhazmat.2019.02.013.

[81] Tanzifi M, Hosseini SH, Kiadehi AD, Olazar M, Karimipour K, Rezaiemehr R, et al. Artificial neural network optimization for methyl orange adsorption onto polyaniline nano-adsorbent: Kinetic, isotherm and thermodynamic studies. Journal of Molecular Liquids 2017;244:189-200. https://doi.org/10.1016/j.molliq.2017.08.122.

[82] Karri RR, Tanzifi M, Tavakkoli Yaraki M, Sahu JN. Optimization and modeling of methyl orange adsorption onto polyaniline nano-adsorbent through response surface methodology and differential evolution embedded neural network. Journal of environmental management 2018;223:517-29. https://doi.org/10.1016/j.jenvman.2018.06.027.

[83] Patra G, Barnwal R, Behera SK, Meikap BC. Removal of dyes from aqueous solution by sorption with fly ash using a hydrocyclone. Journal of Environmental Chemical Engineering 2018;6(4):5204-11. https://doi.org/10.1016/j.jece.2018.08.011.

[84] Liang Y, Li H. A comparison of trimeric surfactant intercalated montmorillonite with its gemini modified one: Characterization and application in methyl orange removal. Journal of Molecular Liquids 2017;227:139-46. https://doi.org/10.1016/j.molliq.2016.11.104.

[85] Saghir S, Xiao Z. Hierarchical mesoporous ZIF-67@LDH for efficient adsorption of aqueous Methyl Orange and Alizarine Red S. Powder Technology 2021;377:453-63. https://doi.org/10.1016/j.powtec.2020.09.006.

[86] Zainal Abidin A, Abu Bakar NHH, Ng EP, Tan WL. Rapid Degradation of Methyl Orange by Ag Doped Zeolite X in the Presence of Borohydride. Journal of Taibah University for Science 2018;11(6):1070-9. https://doi.org/10.1016/j.jtusci.2017.06.004.

[87] Chen Y, Peng J, Xiao H, Peng H, Bu L, Pan Z, et al. Adsorption behavior of hydrotalcite-like modified bentonite for Pb 2+ , Cu 2+ and methyl orange removal from water. Applied Surface Science 2017;420:773-81. https://doi.org/10.1016/j.apsusc.2017.05.138.

[88] Ma Y-z, Zheng D-f, Mo Z-y, Dong R-j, Qiu X-q. Magnetic lignin-based carbon nanoparticles and the adsorption for removal of methyl orange. Colloids and Surfaces A: Physicochemical and Engineering Aspects 2018;559:226-34. https://doi.org/10.1016/j.colsurfa.2018.09.054.

[89] Darwish AAA, Rashad M, Al-Aoh HA. Methyl orange adsorption comparison on nanoparticles: Isotherm, kinetics, and thermodynamic studies. Dyes and Pigments 2019;160:563-71. https://doi.org/10.1016/j.dyepig.2018.08.045.

[90] Jiang B, Jing C, Yuan Y, Feng L, Liu X, Dong F, et al. 2D-2D growth of NiFe LDH nanoflakes on montmorillonite for cationic and anionic dye adsorption performance. J Colloid Interface Sci 2019;540:398-409. https://doi.org/http://dx.doi.org/10.1016/j.jcis.2019.01.022 .

[91] Bhowmik M, Debnath A, Saha B. Fabrication of mixed phase calcium ferrite and zirconia nanocomposite for abatement of methyl orange dye from aqua matrix: Optimization of process parameters. Applied Organometallic Chemistry 2018;32(12):e4607. https://doi.org/10.1002/aoc.4607.

[92] Deka P, Hazarika A, Deka RC, Bharali P. Influence of CuO morphology on the enhanced catalytic degradation of methylene blue and methyl orange. RSC Advances 2016;6(97):95292-305. https://doi.org/10.1039/c6ra20173c.

[93] Li J, Cui H, Song X, Zhang G, Wang X, Song Q, et al. Adsorption and Intercalation of Organic Pollutants and Heavy Metal Ions into MgAl-LDHs Nanosheets with Super High Capacity. RSC Advances 2016:10. https://doi.org/10.1039/C6RA18783H

[94] Blaisi NI, Zubair M, Ihsanullah, Ali S, Kazeem TS, Manzar MS, et al. Date palm ash-MgAl-layered double hydroxide composite: sustainable adsorbent for effective removal of methyl orange and eriochrome black-T from aqueous phase. Environmental science and pollution research international 2018;25(34):34319-31. https://doi.org/10.1007/s11356-018-3367-2.

[95] Liu Q, Liu Q, Wu Z, Wu Y, Gao T, Yao J. Efficient Removal of Methyl Orange and Alizarin Red S from pH-Unregulated Aqueous Solution by the Catechol–Amine Resin Composite Using Hydrocellulose as Precursor. ACS Sustainable Chemistry & Engineering 2017;5(2):1871-80. https://doi.org/10.1021/acssuschemeng.6b02593.

[96] Ling F, Fang L, Lu Y, Gao J, Wu F, Zhou M, et al. A novel CoFe layered double hydroxides adsorbent: High adsorption amount for methyl orange dye and fast removal of Cr(VI). Microporous and Mesoporous Materials 2016;234:230-8. https://doi.org/10.1016/j.micromeso.2016.07.015.

[97] Li J, Zhang S, Chen Y, Liu T, Liu C, Zhang X, et al. A novel three-dimensional hierarchical CuAl layered double hydroxide with excellent catalytic activity for degradation of methyl orange. RSC Advances 2017;7(46):29051-7. https://doi.org/10.1039/c7ra03848h.

[98] Mobarak M, Selim AQ, Mohamed EA, Seliem MK. A superior adsorbent of CTAB/H2O2 solution−modified organic carbon rich-clay for hexavalent chromium and methyl orange uptake from solutions. Journal of Molecular Liquids 2018;259:384-97. https://doi.org/10.1016/j.molliq.2018.02.014.

[99] Pang J, Han Q, Liu W, Shen Z, Wang X, Zhu J. Two basic bismuth nitrates: [Bi6O6(OH)2](NO3)4· 2H2O with superior photodegradation activity for rhodamine B and [Bi6O5(OH)3](NO3)5· 3H2O with ultrahigh adsorption capacity for methyl orange. Applied Surface Science 2017;422:283-94. https://doi.org/10.1016/j.apsusc.2017.06.022.

[100] XinxinYang, Li Y, Gao H, Wang C, Zhang X, Zhou H. One-step fabrication of chitosan-Fe(OH)3 beads for efficient adsorption of anionic dyes. International journal of biological macromolecules 2018;117:30-41. https://doi.org/10.1016/j.ijbiomac.2018.05.137.

[101] He J, Li J, Du W, Han Q, Wang Z, Li M. A mesoporous metal-organic framework: Potential advances in selective dye adsorption. J Alloys Compd 2018;750:360-7. https://doi.org/http://dx.doi.org/10.1016/j.jallcom.2018.03.393.

[102] Ali I, Burakova I, Galunin E, Burakov A, Mkrtchyan E, Melezhik A, et al. High-Speed and High-Capacity Removal of Methyl Orange and Malachite Green in Water Using Newly Developed Mesoporous Carbon: Kinetic and Isotherm Studies. ACS omega 2019;4(21):19293-306. https://doi.org/10.1021/acsomega.9b02669.

[103] Znad H, Abbas K, Hena S, Awual MR. Synthesis a novel multilamellar mesoporous TiO2/ZSM-5 for photo-catalytic degradation of methyl orange dye in aqueous media. Journal of Environmental Chemical Engineering 2018;6(1):218-27. https://doi.org/10.1016/j.jece.2017.11.077.

[104] Li S, Jia Z, Li Z, Li Y, Zhu R. Synthesis and characterization of mesoporous carbon nanofibers and its adsorption for dye in wastewater. Adv Powder Technol 2016;27(2):591-8. https://doi.org/http://dx.doi.org/10.1016/j.apt.2016.01.024.

[105] Deb A, Kanmani M, Debnath A, Bhowmik KL, Saha B. Ultrasonic assisted enhanced adsorption of methyl orange dye onto polyaniline impregnated zinc oxide nanoparticles: Kinetic, isotherm and optimization of process parameters. Ultrasonics sonochemistry 2019;54:290-301. https://doi.org/10.1016/j.ultsonch.2019.01.028.

[106] Istratie R, Stoia M, Păcurariu C, Locovei C. Single and simultaneous adsorption of methyl orange and phenol onto magnetic iron oxide/carbon nanocomposites. Arabian Journal of Chemistry 2019;12(8):3704-22. https://doi.org/10.1016/j.arabjc.2015.12.012.

[107] Li X, Yuan H, Quan X, Chen S, You S. Effective adsorption of sulfamethoxazole, bisphenol A and methyl orange on nanoporous carbon derived from metal-organic frameworks. J Environ Sci (China) 2018;63:250-9. https://doi.org/10.1016/j.jes.2017.10.019.

[108] Ba Mohammed B, Lgaz H, Alrashdi AA, Yamni K, Tijani N, Dehmani Y, et al. Insights into methyl orange adsorption behavior on a cadmium zeolitic-imidazolate framework Cd-ZIF-8: A joint experimental and theoretical study. Arabian Journal of Chemistry 2021;14(1):102897. https://doi.org/10.1016/j.arabjc.2020.11.003.

[109] Sun B, Yuan Y, Li H, Li X, Zhang C, Guo F, et al. Waste-cellulose-derived porous carbon adsorbents for methyl orange removal. Chemical Engineering Journal 2019;371:55-63. https://doi.org/10.1016/j.cej.2019.04.031.

[110] Tripathy N, Ahmad R, Kuk H, Lee DH, Hahn YB, Khang G. Rapid methyl orange degradation using porous ZnO spheres photocatalyst. Journal of photochemistry and photobiology B, Biology 2016;161:312-7. https://doi.org/10.1016/j.jphotobiol.2016.06.003.

[111] Kang D, Yu X, Ge M, Xiao F, Xu H. Novel Al-doped carbon nanotubes with adsorption and coagulation promotion for organic pollutant removal. J Environ Sci (China) 2017;54:1-12. https://doi.org/10.1016/j.jes.2016.04.022.

[112] Kundu S, Chowdhury IH, Naskar MK. Synthesis of hexagonal shaped nanoporous carbon for efficient adsorption of methyl orange dye. Journal of Molecular Liquids 2017;234:417-23. https://doi.org/10.1016/j.molliq.2017.03.090.

[113] Martini BK, Daniel TG, Corazza MZ, de Carvalho AE. Methyl orange and tartrazine yellow adsorption on activated carbon prepared from boiler residue: Kinetics, isotherms, thermodynamics studies and material characterization. Journal of Environmental Chemical Engineering 2018;6(5):6669-79. https://doi.org/10.1016/j.jece.2018.10.013.

[114] Chen Y, Jing C, Zhang X, Jiang D, Liu X, Dong B, et al. Acid-salt treated CoAl layered double hydroxide nanosheets with enhanced adsorption capacity of methyl orange dye. J Colloid Interface Sci 2019;548:100-9. https://doi.org/10.1016/j.jcis.2019.03.107.

[115] Albayati TM, Alwan GM, Mahdy OS. High performance methyl orange capture on magnetic nanoporous MCM-41 prepared by incipient wetness impregnation method. Korean Journal of Chemical Engineering 2016;34(1):259-65. https://doi.org/10.1007/s11814-016-0231-2.

[116] Ibrahim RK, El-Shafie A, Hin LS, Mohd NSB, Aljumaily MM, Ibraim S, et al. A clean approach for functionalized carbon nanotubes by deep eutectic solvents and their performance in the adsorption of methyl orange from aqueous solution. Journal of environmental management 2019;235:521-34. https://doi.org/10.1016/j.jenvman.2019.01.070.

[117] Li H, An N, Liu G, Li J, Liu N, Jia M, et al. Adsorption behaviors of methyl orange dye on nitrogen-doped mesoporous carbon materials. J Colloid Interface Sci 2016;466:343-51. https://doi.org/10.1016/j.jcis.2015.12.048.

[118] Shen J, Wang X, Zhang L, Yang Z, Yang W, Tian Z, et al. Size-selective adsorption of methyl orange using a novel nano-composite by encapsulating HKUST-1 in hyper-crosslinked polystyrene networks. Journal of Cleaner Production 2018;184:949-58. https://doi.org/10.1016/j.jclepro.2018.03.015.

[119] Zayed AM, Abdel Wahed MSM, Mohamed EA, Sillanpää M. Insights on the role of organic matters of some Egyptian clays in methyl orange adsorption: Isotherm and kinetic studies. Applied Clay Science 2018;166:49-60. https://doi.org/10.1016/j.clay.2018.09.013.

[120] Bhowmik M, Deb K, Debnath A, Saha B. Mixed phase Fe2O3/Mn3O magnetic nanocomposite for enhanced adsorption of methyl orange dye: Neural network modeling and response surface methodology optimization. Applied Organometallic Chemistry 2017;32(3):e4186. https://doi.org/10.1002/aoc.4186.

[121] Mokhtari P, Ghaedi M, Dashtian K, Rahimi MR, Purkait MK. Removal of methyl orange by copper sulfide nanoparticles loaded activated carbon: Kinetic and isotherm investigation. Journal of Molecular Liquids 2016;219:299-305. https://doi.org/10.1016/j.molliq.2016.03.022.

[122] Chowdhury A, Kumari S, Khan AA, Hussain S. Selective removal of anionic dyes with exceptionally high adsorption capacity and removal of dichromate (Cr2O7(2-)) anion using Ni-Co-S/CTAB nanocomposites and its adsorption mechanism. J Hazard Mater 2020;385:121602. https://doi.org/10.1016/j.jhazmat.2019.121602.

[123] Liu X, Tian J, Li Y, Sun N, Mi S, Xie Y, et al. Enhanced dyes adsorption from wastewater via Fe3O4 nanoparticles functionalized activated carbon. J Hazard Mater 2019;373:397-407. https://doi.org/10.1016/j.jhazmat.2019.03.103.

[124] Rekha P, Muhammad R, Sharma V, Ramtekeb M, Paritosh Mohanty P. Unprecedented adsorptive removal of Cr2O7 by a low surface area organosilica. Journal of Materials Chemistry A 2016:9. https://doi.org/10.1039/C6TA08940B

[125] Yu Y, Qiao N, Wang D, Zhu Q, Fu F, Cao R, et al. Fluffy honeycomb-like activated carbon from popcorn with high surface area and well-developed porosity for ultra-high efficiency adsorption of organic dyes. Bioresour Technol 2019;285:121340. https://doi.org/10.1016/j.biortech.2019.121340.

[126] Islam MS, Ang BC, Gharehkhani S, Afif ABM. Adsorption capability of activated carbon synthesized from coconut shell. Carbon Letters 2016;20:9. https://doi.org/10.5714/CL.2016.20.001.

[127] Alhaji NMI, Nathiya D, Kaviyarasu K, Meshram M, Ayeshamariam A. A comparative study of structural and photocatalytic mechanism of AgGaO2 nanocomposites for equilibrium and kinetics evaluation of adsorption parameters. Surfaces and Interfaces 2019;17:100375. https://doi.org/10.1016/j.surfin.2019.100375.

[128] Saeed M, Adeel S, Ilyas M, Shahzad MA, Usman M, Haq E-u, et al. Oxidative degradation of Methyl Orange catalyzed by lab prepared nickel hydroxide in aqueous medium. Desalination and Water Treatment 2015;57(27):12804-13. https://doi.org/10.1080/19443994.2015.1052992.

[129] Shen Z, Zhou H, Chen H, Xu H, Feng C, Zhou X. Synthesis of Nano-Zinc Oxide Loaded on Mesoporous Silica by Coordination Effect and Its Photocatalytic Degradation Property of Methyl Orange. Nanomaterials 2018;8(5). https://doi.org/10.3390/nano8050317.

[130] Tanhaei B, Ayati A, Lahtinen M, Vaziri BM, Sillanp€a M. A magnetic mesoporous chitosan based core-shells biopolymer for anionic dye adsorption Kinetic and isothermal study and application of ANN. Journal of Applied Polymer Science 2016:11. https://doi.org/10.1002/app.43466

[131] Shi J, Kuwahara Y, An T, Yamashita H. The fabrication of TiO2 supported on slag-made calcium silicate as low-cost photocatalyst with high adsorption ability for the degradation of dye pollutants in water. Catalysis Today 2017;281:21-8. https://doi.org/10.1016/j.cattod.2016.03.039.

[132] Gupta K, Gupta D, Khatri OP. Graphene-like porous carbon nanostructure from Bengal gram bean husk and its application for fast and efficient adsorption of organic dyes. Applied Surface Science 2019;476:647-57. https://doi.org/10.1016/j.apsusc.2019.01.138.

[133] Li H, Sun Z, Zhang L, Tian Y, Cui G, Yan S. A cost-effective porous carbon derived from pomelo peel for the removal of methyl orange from aqueous solution. Colloids and Surfaces A: Physicochemical and Engineering Aspects 2016;489:191-9. https://doi.org/10.1016/j.colsurfa.2015.10.041.

[134] Hasan M, Rashid MM, Hossain MM, Al Mesfer MK, Arshad M, Danish M, et al. Fabrication of polyaniline/activated carbon composite and its testing for methyl orange removal: Optimization, equilibrium, isotherm and kinetic study. Polymer Testing 2019;77:105909. https://doi.org/10.1016/j.polymertesting.2019.105909.

[135] da Silva RJ, Mojica-Sanchez LC, Gorza FDS, Pedro GC, Maciel BG, Ratkovski GP, et al. Kinetics and thermodynamic studies of Methyl Orange removal by polyvinylidene fluoride-PEDOT mats. J Environ Sci (China) 2021;100:62-73. https://doi.org/10.1016/j.jes.2020.04.034.

[136] Arshadi M, Mousavinia F, Amiri MJ, Faraji AR. Adsorption of methyl orange and salicylic acid on a nano-transition metal composite: Kinetics, thermodynamic and electrochemical studies. J Colloid Interface Sci 2016;483:118-31. https://doi.org/10.1016/j.jcis.2016.08.032.

[137] Lu Y, Jiang B, Fang L, Ling F, Gao J, Wu F, et al. High performance NiFe layered double hydroxide for methyl orange dye and Cr(VI) adsorption. Chemosphere 2016;152:415-22. https://doi.org/10.1016/j.chemosphere.2016.03.015.

[138] Abo El Naga AO, Shaban SA, El Kady FYA. Metal organic framework-derived nitrogen-doped nanoporous carbon as an efficient adsorbent for methyl orange removal from aqueous solution. Journal of the Taiwan Institute of Chemical Engineers 2018;93:363-73. https://doi.org/10.1016/j.jtice.2018.07.044.

[139] Ahmadijokani F, Mohammadkhani R, Ahmadipouya S, Shokrgozar A, Rezakazemi M, Molavi H, et al. Superior

chemical stability of UiO-66 metal-organic frameworks (MOFs) for selective dye adsorption. Chem Eng J 2020;399:125346. https://doi.org/http://dx.doi.org/10.1016/j.cej.2020.125346.

[140] Chen X, Wu Z, Gao Z, Ye BC. Effect of Different Activated Carbon as Carrier on the Photocatalytic Activity of Ag-N-ZnO Photocatalyst for Methyl Orange Degradation under Visible Light Irradiation. Nanomaterials 2017;7(9). https://doi.org/10.3390/nano7090258.

[141] Leal Marchena C, Lerici L, Renzini S, Pierella L, Pizzio L. Synthesis and characterization of a novel tungstosilicic acid immobilized on zeolites catalyst for the photodegradation of methyl orange. Applied Catalysis B: Environmental 2016;188:23-30. https://doi.org/10.1016/j.apcatb.2016.01.064.

[142] Zhang B, Wu Y, Cha L. Removal of methyl orange dye using activated biochar derived from pomelo peel wastes: performance, isotherm, and kinetic studies. Journal of Dispersion Science and Technology 2019;41(1):125-36. https://doi.org/10.1080/01932691.2018.1561298.

[143] Wu S-c, Yu L-l, Xiao F-f, You X, Yang C, Cheng J-h. Synthesis of aluminum-based MOF/graphite oxide composite and enhanced removal of methyl orange. Journal of Alloys and Compounds 2017;724:625-32. https://doi.org/10.1016/j.jallcom.2017.07.095.

[144] Tella AC, Olawale MD, Neuburger M, Obaleye JA. Synthesis and crystal structure of Cd-based metal-organic framework for removal of methyl-orange from aqueous solution. Journal of Solid State Chemistry 2017;255:157-66. https://doi.org/10.1016/j.jssc.2017.07.019.

[145] Borsagli FGLM, Ciminelli VST, Ladeira CL, Haas DJ, Lage AP, Mansur HS. Multi-functional eco-friendly 3D scaffolds based on N-acyl thiolated chitosan for potential adsorption of methyl orange and antibacterial activity against Pseudomonas aeruginosa. Journal of Environmental Chemical Engineering 2019;7(5):103286. https://doi.org/10.1016/j.jece.2019.103286.

[146] Qi X, Wu L, Su T, Zhang J, Dong W. Polysaccharide-based cationic hydrogels for dye adsorption. Colloids and surfaces B, Biointerfaces 2018;170:364-72. https://doi.org/10.1016/j.colsurfb.2018.06.036.

[147] Albayati TM. Application of nanoporous material MCM-41 in a membrane adsorption reactor (MAR) as a hybrid process for removal of methyl orange. Desalination and Water Treatment 2019;151:138-44. https://doi.org/10.5004/dwt.2019.23878.